A shear compression disk specimen with controlled stress triaxiality under quasi-static loading

Dorogoy[(1*)] A., Karp[(2)] B. and Rittel[(1)] D.

[(1)] *Faculty of Mechanical Engineering, Technion – Israel Institute of Technology, 32000 , Haifa, Israel.*

[(2)] *Department of Mechanical Engineering, Ben-Gurion University of the Negev, P.O.B. 653, Beer-Sheva 84105, Israel.*

Abstract

This paper introduces a double shear axisymmetric specimen (Shear Compression Disk) and the methodology to extract flow and fracture properties of ductile materials, under various stress triaxiality levels. A thorough numerical investigation of the experimental set-up is performed, which reveals that the stresses are quite uniformly distributed in the gauge section during all the stages of the test. The attainable level of stress triaxiality (with pressures of up to 1.9 GPa) ranges from -0.1 to 1, which can be adjusted by a proper choice of geometrical parameters of the specimen.
The methodology is implemented to quasi-static experiments on 4340 Steel and Aluminum 7075-T651 specimens. The flow properties are compared to those obtained by upsetting cylinders and show a very good agreement. For these materials it is observed that, contrary to the fracture strain, the flow properties are quite insensitive to the level of stress triaxiality. The fracture strain of the aluminum alloy increases with triaxiality and may be fitted with an exponential polynomial of the type suggested by Johnson and Cook (1985). These examples demonstrate the potential of the new specimen to obtain flow and fracture properties of ductile materials under controlled triaxiality.

Keywords: a. triaxiality . b. ductile fracture. c.flow properties. d. finite elements. e. quasi-static loading

*Corresponding author.Tel.:+97248292236.
E-mail address: dorogoy@technion.ac.il

1. Introduction

The modern engineering environment generates a constant need for improved design procedures based on new materials. These requirements pose a great challenge for a sophisticated characterization of plasticity and failure of materials under complex loading. In particular, most of "high performance" applications expose the materials to extreme conditions requiring an accurate material characterization taking into account the stress triaxiality and strain rate effects (e.g., Che *et al.*, 2007). It is well accepted that the common criteria for yield (e.g., Tresca or von-Mises) and ductile fracture (e.g., Gurson), which are all used to transpose the one-dimensional experimental results to triaxial conditions, are only rough approximations for material plasticity and fracture (Yu, 2004). Reliance on these bounds for high strain-rate conditions is based on the abundance of one-dimensional experimental data on material properties, using various specimen geometries beyond the classical tensile/compression ones, such as the Shear Compression Specimen (Rittel *et al.* 2002, Dorogoy and Rittel, 2005), the hat-shaped specimen (e.g., Meyer and Manwaring, 1986, Couque, 2003, Couque, 2005, Gua and Nesterenko, 2007, Mishra *et al.*, 2008), the double-shear specimen (Rusinek and Klepaczko, 2001, Li and Jones, 2002,), the punch specimen (Guduru *et al.*, 2007) and the butterfly specimens (Mae, 2009). All these geometries are used in both quasi-static and dynamic loading configurations. Since failure of ductile materials is well-known to depend on the degree of stress triaxiality (Bridgman, 1952), these specimen geometries provide only a partial characterization of the material behavior.

Yet, several specimen geometries can be found for specific experimental investigation of triaxiality effect. Among the more common configurations are a circumferentially-notched tensile specimen (e.g., Hancock & Mackenzie, 1976, Hopperstad et al., 2003, Mirone, 2007), notched plane specimens (e.g., Mirone, 2008), shear and plane-notched tensile specimens (e.g., Brünig et al., 2008), and a standard tensile specimen exposed to hydrostatic compression in a chamber (Larose and Lewandowski, 2002). These experiments are used to extract a variety of properties including plastic behavior and fracture strain. Some of the specimens are used also under

dynamic loading (Alves and Jones, 1999, Che et al., 2007). An authoritative review of results of these investigations can be found in Lewandowski and Lowhaphandu (1998).

Each of these specimens introduces a limit on some of the desirable characteristics of the experimental configuration, such as, large non-uniformity of stress in the gauge region, non-constant triaxiality level during the loading, limited range of triaxiality, heavy reliance on numerical analysis for experimental interpretation. Though altogether, these specimens provide a large variety of stress combinations, this large diversity may inhibit the derivation of a consistent model for material behavior from early plasticity up to failure under triaxial stress-state and high strain-rate conditions.

The purpose of the present paper is to present an experimental and numerical study of the development of a new specimen configuration which allows for the investigation of stress triaxiality effect on flow and fracture behavior of ductile materials. The configuration of the specimen is inspired from the Double-Shear specimen, which was suggested decades ago by Fergusson et al. (1967) and later revisited by Klepaczko (1998). The main characteristics of the new specimen, referred here as the Shear Compression Disk (SCD), are as follows:

1. Shear is the dominant loading mode of the material as appropriate for plasticity study.
2. Easy control over the level of the normal stresses (or pressure) on the sheared section (including both positive and negative).
3. Small and easy to manufacture.
4. Same specimen geometry to be used for quasi-static (reported here) and dynamic experiments (work in progress).
5. Simple experimental procedure and interpretation.
6. Reasonably high range of *triaxiality* (tr) range, $t_r = \dfrac{\sigma_m}{\hat{\sigma}_{eq}}$, where the effective *pressure* is defined by $\sigma_m = -\dfrac{1}{3}\sigma_{ii}$ and $\hat{\sigma}_{eq}$ is the equivalent von Mises stress.

The numerical analysis of the experimental set up shows a relatively uniform stress distribution within the gauge area, within a wide range of triaxiality $-0.2 < t_r < 1.2$ (for large strains). The level of the triaxiality during the main load step can be made to

vary or remain rather constant during the test. This is done by choosing the proper design parameters which fit the experimental requirements.

This paper introduces the specimen, its numerical modeling and data reduction procedures, followed by preliminary experimental results obtained for 4340 steel and Aluminum 7075 T651 specimens. This work describes the basic features related to quasi-static experiments, while dynamic testing will be reported in a separate paper.

2. The specimen and experimental setup

2.1 The experimental set-up

The setup consists of three elements: (1) Confining holder, (2) Specimen and (3) Spacing ring. These components are shown in Fig. 1 in exploded and assembled views. The confining holder and the spacing ring are used to achieve the required pre-set stress within the specimen gauge area. The inner surface of the confining holder is inclined to the specimen's basis by an angle α matching the inclination of the conical outer surface of the specimen (Fig. 2a). Upon forced insertion of the specimen into the holder, confining stresses are generated in the specimen. The magnitude of the stresses depends on the angle α and the insertion distance Δ (Fig. 2a). The spacing ring is used to set and limit, if necessary, the insertion distance Δ.

2.2 Specimen geometry

The basic configuration of the specimen is inspired from the double shear (DS) specimen (Klepaczko, 1998), with two main modifications in order to control the hydrostatic pressure level within the gauge.

The first modification consists of selecting a truncated cone specimen of half angle $90^{\circ} - \alpha$ (Fig. 2a). This inclination is aimed at generating pressure in the sheared gauge section *prior to the application of main load* (to be detailed below).

The second modification concerns the inclination β of the slot defining the gauge area (Fig. 2a). This inclination, together with the insertion distance, serves as a control over

the stress triaxiality of the test. The two angles of inclination, α and β, and the insertion distance, Δ, are design parameters whose effect is analyzed in section 3.

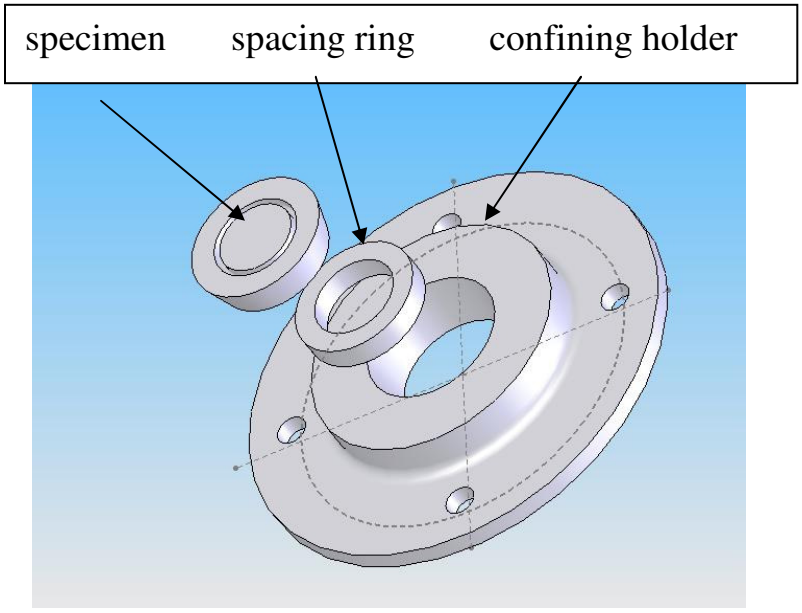

a.

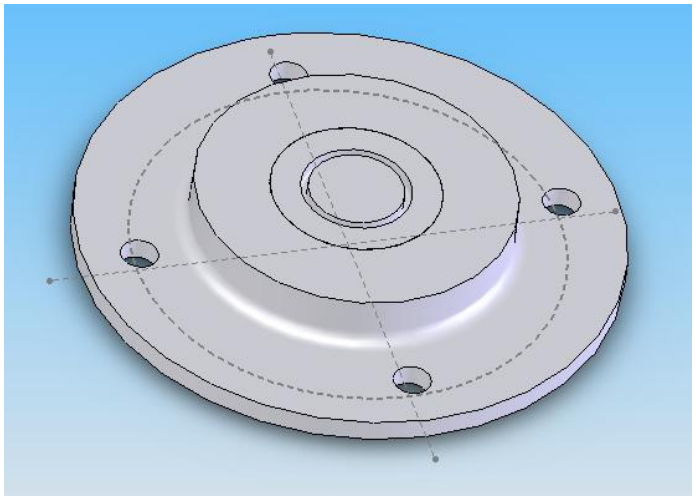

b.

Figure 1: The experimental setup. a. Before assembly. b. After assembly. Note that the upper face of the cylinder and the specimen are on the same level after assembly.

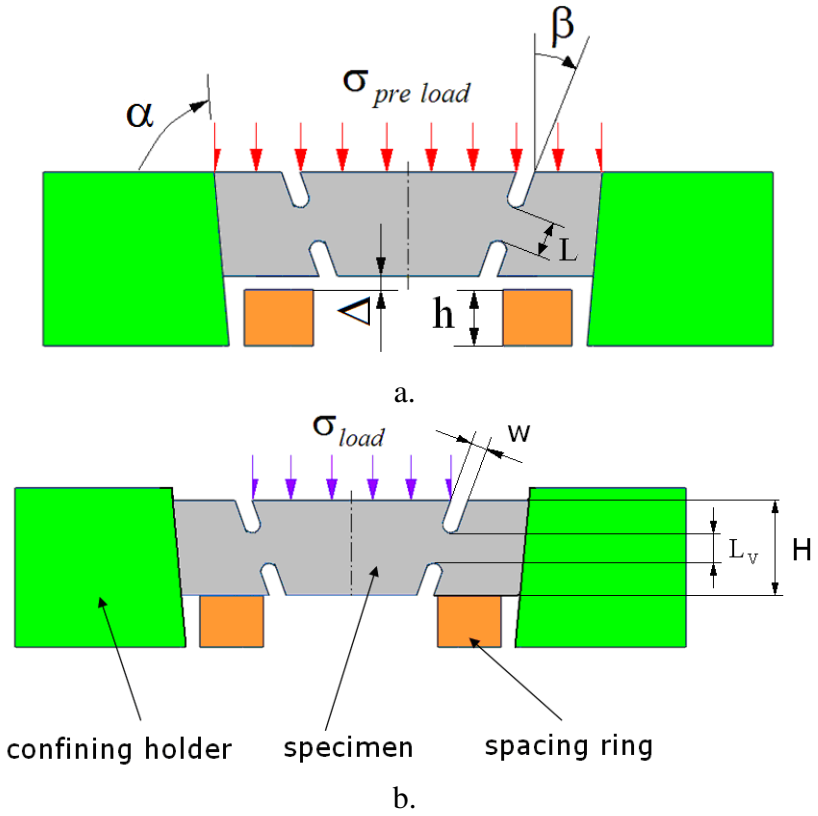

Figure 2: The experimental setup. a. Position in the pre-set stage. b. Position at the main loading path.

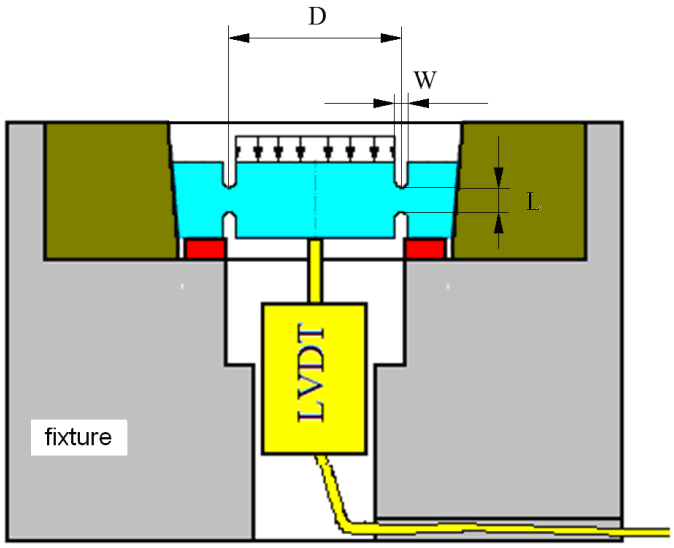

Figure 3: Schematic cut view of the experimental setup.

2.3 Experimental procedure

The experiment is performed in two steps.

1. The first step, referred here to as "*pre-set*", consists of insertion of the specimen into the holder up to a distance Δ predetermined by the height *h* of the spacing ring. The conical contact surface between the specimen and the holder is lubricated to decrease the applied force required for specimen insertion. This step introduces stresses within the specimen, whose magnitude depends on the angle α, insertion distance Δ, and also on the material properties of the specimen and those of the confining holder.

2. The second step, "*main loading*", consists of application of a uniform load on the inner disk of the specimen as shown in Fig. 2b. The measured quantities which represent the main loading path are the load and the displacement of the inner part of the specimen. A special fixture was designed for attachment of an LVDT to accurately measure the displacement of the bottom face of the specimen in both pre-set and main-loading steps. The complete setup, in a configuration ready for the second experimental step, is shown in Fig. 3.

3. The stress triaxiality level

For a confining cylinder made of known material (maraging steel), the level of stress triaxiality within the gauge during the main loading step is controlled by the three parameters α, β, and Δ (Fig. 2a). The initial triaxiality is mainly dictated by α and Δ, while β dictates its evolution during the main loading step. In the present study a fixed angle $\alpha = 85^{o}$ has been chosen. For the case of $\beta = 0$, the main loading mode is primarily shear with a transition to tension at large levels of deformation, similar to the original double shear plane stress specimen (Klepaczko, 1998). A numerical investigation is performed to study the effect of β and Δ on the evolution of local and average triaxiality within the gauge during the main loading step.

Five distinct values of β were examined: -10^o, 0^o, 10^o, 20^o and 30^o combined with two values of $\Delta = 0.0, 0.75$ mm. Only the value of $\Delta = 0.0$ mm was examined for $\beta = -10^o$ to characterize the development of a negative pressure.

The numerical procedure and results are shown next. The results are sub-grouped in the following sequence: 1) Plastic strain distribution within the gauge. 2) Uniformity of triaxiality within the gauge. 3) Effect of β on the evolution of the average triaxiality during loading. 4) Effect of Δ on the triaxiality (two values $\Delta = 0.0, 0.75$ mm) for each β .

3.1 Numerical Scheme

Numerical simulations were been used here for two main purposes: to evaluate the degree of stress homogeneity within the gauge (which should facilitate proper extraction of material properties), and to assist in the interpretation of the experimental results.

The axisymmetric meshed models which correspond to the two extreme β values are shown in Fig. 4. The upper inner diameter is 12.7 mm while the upper outer diameter is 22.7 mm. The slot width w=1.0 mm and the gauge vertical length L_v= 2 mm. The specimen overall height is H=6 mm and its outer faces are inclined by $\alpha = 85^o$, as shown in figure 2a,b. An axi-symmetric analysis was conducted with Abaqus Standard 6.9 EF1. Quadratic quadrilateral elements of type CAX8 were used. The size of the elements in the gauge is ~2.5% of the gauge length. The analysis for pre loaded specimens was conducted in three steps. In the first step (1) a displacement Δ was applied all along the upper face of the specimen. In the second step (2) the load was relieved. The third step (3) consisted of applying a displacement of 0.5 mm on the inner disk of the upper face of the specimen. For the specimens with $\Delta = 0$ only the third step was applied. This third step was also applied to the specimen with -10^o inclination of the slot, since a negative pressure was pursued. A frictional contact with Coloumb coefficient of friction (cof) of 0.1 was assumed between all contacting surfaces. This cof is typical of well lubricated contacting metal surfaces. The 4340 steel was modeled as a bi-linear elastic-plastic material model with Ep = 0.4 GPa. The elastic properties which were used are: Young's modulus $E = 210\ GPa$, Poisson's ratio $\nu = 0.3$ and yield stress $\sigma_y = 1400$ MPa.

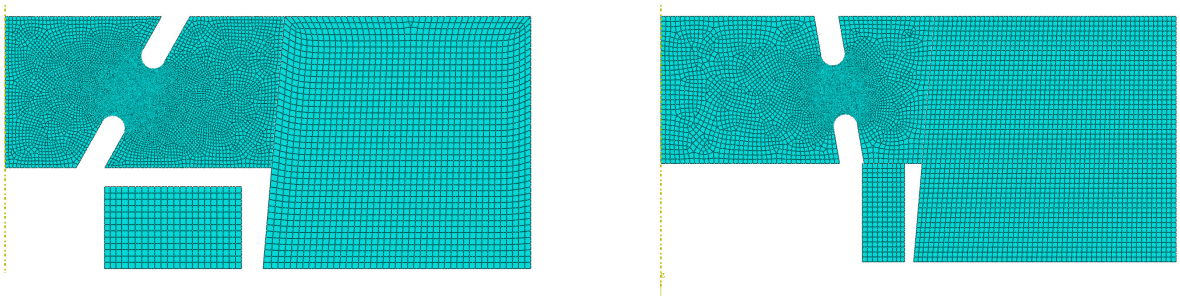

a. b.

Figure 4: Meshed axi-symmetric models which were used in the numerical scheme. a. 30^o inclination. Note the gap ready for pre-load step of the experiment. b. -10^o inclination. Note that the gap is closed, ready for the main load step of the experiment.

3.2 Pre-set

The main purpose of the pre-set is to induce various triaxiality levels within the gauge prior to execution of the main loading step. For a pre-determined angle α, the level of initial triaxiality is determined by Δ. For the particular materials investigated here (4340 and 7075), it was estimated that the maximal value that will induce only minimal yield within the gauge corresponds to $\Delta = 0.75$ mm. The resulting residual strain and pressure for that case are detailed here.

The distribution of the residual pressure within the gauge after the load release (numerical step 2) for 4340 specimens with $\beta = 0^o$ and $\beta = 30^o$ is shown in Figs. 5a and 5b respectively. Some stress concentration near the slot tips is evident, as expected. The light (green) color represents a pressure of ~600 MPa while in the darker (red) areas, the pressure might reach a peak value of 1200 MPa. While these concentrations lie on the "working line" (showed as a thick purple line) for $\beta = 0^o$, they lie outside this line for $\beta = 30^o$. This behavior implies that the uniformity of the initial stress distribution in the gauge along the working line is better for a non-zero β. The plastic strain distribution within the gauge after the load release (step 2) for a specimens with $\beta = 0^o$ and $\beta = 30^o$ is shown in Figs. 5c and 5d respectively. It can be observed that only very small part of the gauge undergoes plastic deformation during the pre set (step 1). For $\beta = 30^o$ these small plastic zones are outside the working line of the gauge.

The question of uniformity will be further examined for the various combinations of Δ and β in the sequel.

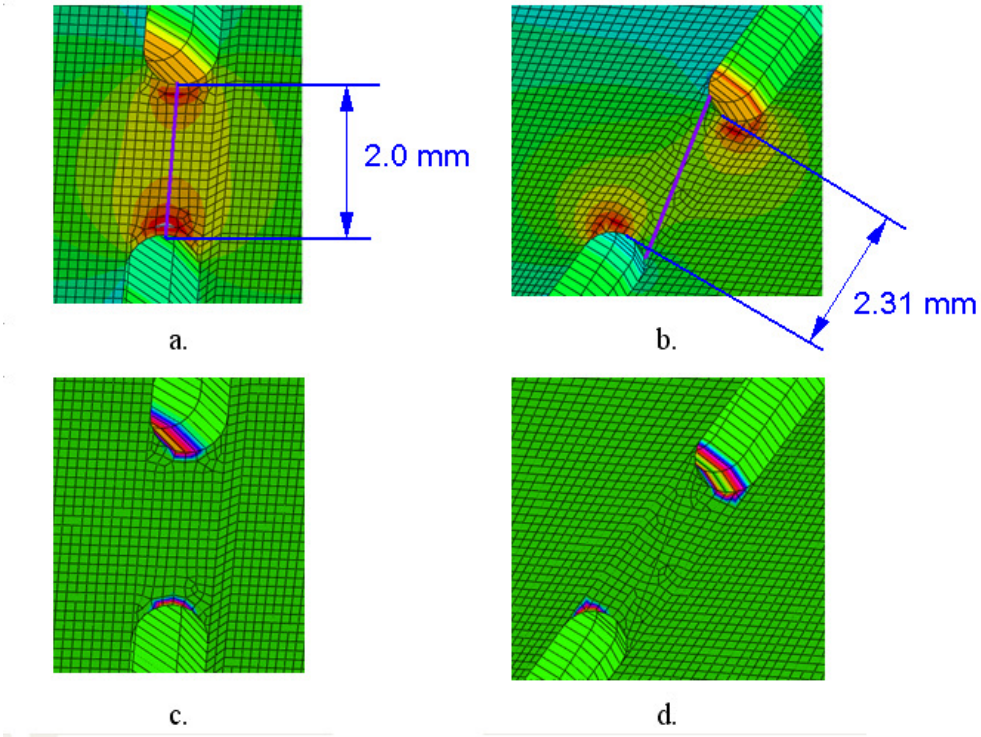

Figure 5: Pre set effects due to Δ = 0.75 mm. a. Residual stress for β = 0°. b. Residual pressure for β = 30°. c. Residual plastic strain for β = 0° . d. Residual plastic strain for β = 30°. Note the paths on figures a and b on which field values of the neighboring elements were used for averaging purposes.

3.3 Main loading step

3.3.1 Stress uniformity within the gauge area

To check the uniformity of stress triaxiality during the main loading step, as well as the effect of the pre-set Δ, the equivalent von Mises stress $\sigma_{eq}(\hat{x})$ and the mean stress $P(\hat{x})$ were extracted along the sheared surfaces, whose paths are shown in Figs. 5a,b.

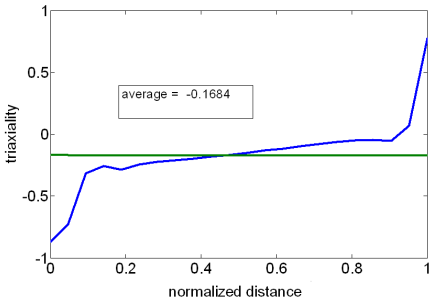

a.

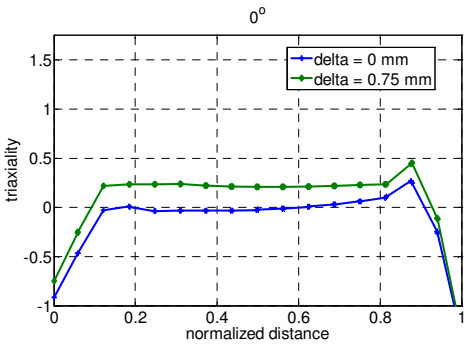

b.

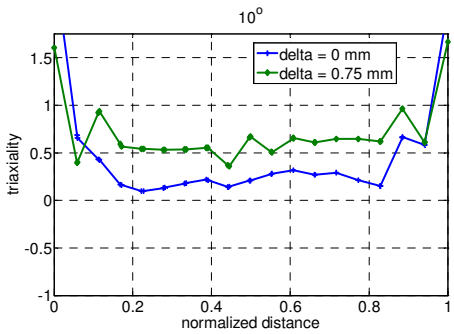

c.

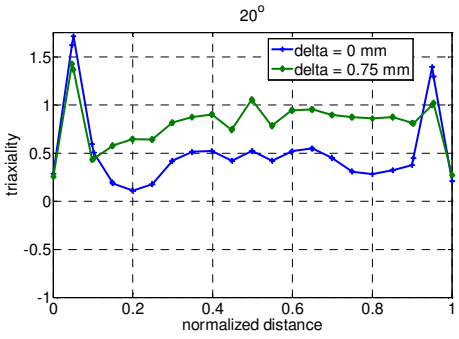

d.

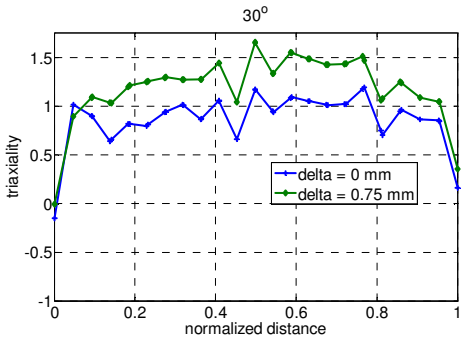

e.

Figure 6: The distribution of the triaxiality along the paths of Fig. 7 for two values of pre set $\Delta = 0.0$ mm and $\Delta = 0.75$ mm. a. $\beta = -10^o$. b. $\beta = 0^o$. c. $\beta = 10^o$. d. $\beta = 20^o$. e. $\beta = 30^o$.

The symbol $\hat{x} = x / L$ represents the normalized distance along the gauge length which is the abscissa of Figs. 6. The path starts at the bottom of the gauge and ends at its top. The values are obtained for the elements along the paths at a specific $\hat{\varepsilon}_p$. For $\beta = -10^o$, $\hat{\varepsilon}_p = 0.1$, while for all other values of β, the equivalent plastic strain lies in the range $0.25 \le \hat{\varepsilon}_p \le 0.33$. For $\beta = -10^o$ the strain $\hat{\varepsilon}_p$ is smaller because the fracture strain for a

negative pressure is smaller. The stress triaxiality for $\beta = -10^o$ is shown in Fig. 6a. The stress triaxialities for $\beta = -10^o$, 0^o, 10^o, 20^o and 30^o are shown in Figs. 6a-6e. The results show a consistent level of uniformity in the range $0.15 \le \hat{x} \le 0.85$ while close to the specimen's slot tips $(\hat{x} < 0.15,\ \hat{x} > 0.85)$, the triaxiality differs most likely because of local stress concentration effects. Fig. 6 also shows that the pre-set causes a consistent increase in stress triaxiality, thus providing a convenient means for controlling it.

3.3.2 Gauge deformation and plastic strain at a specified load

The gauge deformation and plastic strain contour maps after pre-set (1), release (2) and main loading step (3) are shown in Figs. 7b-7f . Fig. 7a shows the color contour map of the plastic strains. The pre set $\Delta = 0.0$ mm was applied to the specimen with $\beta = -10^o$ (Fig. 7b) while a pre set of $\Delta = 0.75$ mm was applied to specimens with $\beta = 0^o$, 10^o, 20^o and 30^o which are shown in Figs. 7c - 7f respectively.

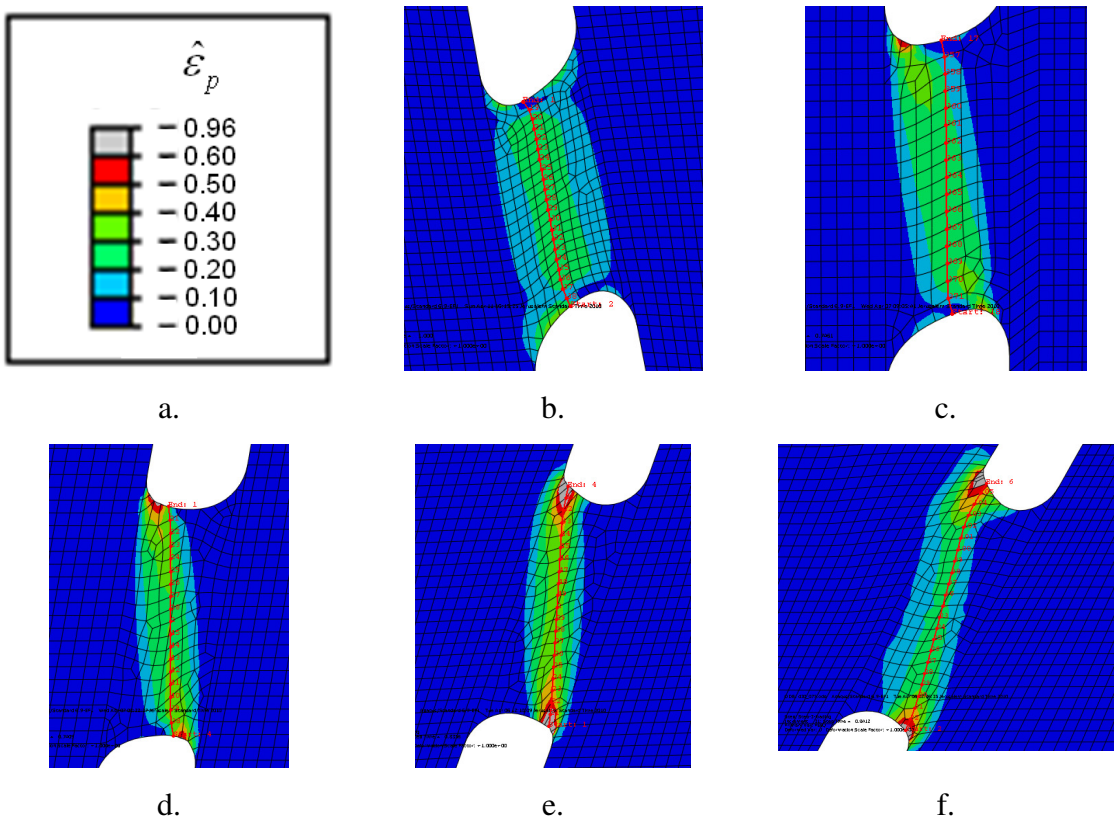

a. b. c.

d. e. f.

Figure 7: Load effects on the deformed gauge and the equivalent plastic strain($\hat{\varepsilon}_p$) distribution. a. Color contour map of $\hat{\varepsilon}_p$. b. β = -10^o , Δ = 0.0 mm and $\hat{\varepsilon}_p$ = 0.1. c. β = -0.0^o , Δ = 0.75 mm and $\hat{\varepsilon}_p$ = 0.25. d. β = 10^o , Δ = 0.75 mm and $\hat{\varepsilon}_p$ = 0.27. e. β = 20^o , Δ = 0.75 mm and $\hat{\varepsilon}_p$ = 0.27. d. β = 30^o , Δ = 0.75 mm and $\hat{\varepsilon}_p$ = 0.33.

In each of the figures 7b-7f, a path which lies within the working zone of the gauge is shown. The average stresses and strains which are calculated along this path are representative of those in the gauge area. A "history output" along this path was obtained. This output includes time dependent values of stresses and strains at all integration points of the elements along these paths. The average value of the plastic strain (for example) of all the integration points within the elements adjacent to the path represents the average value within the working part of the gauge. Figs. 7b-7f are plotted at an average value of strains: $\hat{\varepsilon}_p$ = 0.1, 0.25, 0.27, 0.27 and 0.33 respectively.

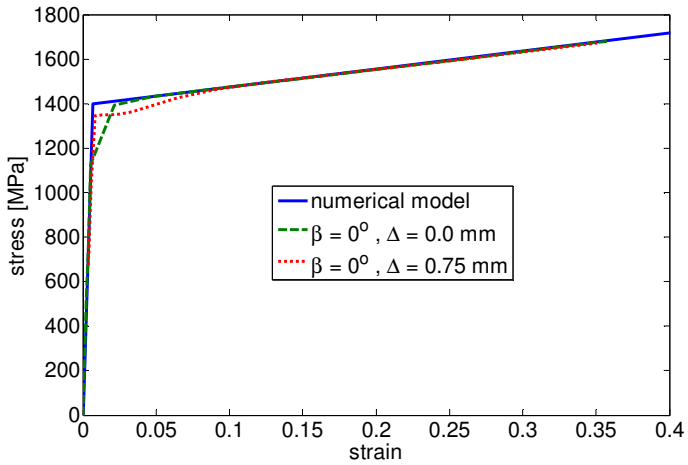

Figure 8: Averaged stress-stress curves along the path in comparison to the applied material model for specimens of $\beta = 0^0$ without pre-load and with pre load of $\Delta = 0.75$ *mm*

The numerical simulations showed that the averaged stresses and strains along the paths shown in Fig. 7 closely reproduce the prescribed material model. Fig. 8 shows for example the averaged stress-stress curves along the path in comparison to the applied material model. Here, $\beta = 0^0$ and for two load cases of $\Delta = 0.0$ *mm* (no pre-load step (1)), and with pre load step (1) of $\Delta = 0.75$ *mm*. Some small discrepancies are evident

close to yield point and up to 7% true strain. For larger strains the agreement is excellent. This result indicates that for a specific specimen and known material properties, the applied displacements and load (d-P) can be mapped onto the averaged von Mises stress and equivalent strain $(\hat{\sigma},\hat{\varepsilon})$ in the gauge which represent well the material model. A similar technique is used with the SCS specimens (Dorogoy and Rittel, 2005). Linear data reduction formulas for strains and stresses above the yield point (ie $\hat{\varepsilon} > \varepsilon_y$; $\hat{\sigma} > \sigma_y$) can be written as:

$$\hat{\varepsilon} = \varepsilon_y + \frac{k_1 d_y}{w}\left(\frac{d}{d_y} - 1\right) \tag{1}$$

$$\hat{\sigma} = \sigma_y + \sigma_y k_2\left(\frac{P}{P_y} - 1\right) \tag{2}$$

The coefficients k_1 and k_2 are determined numerically for a specific specimen and material model, where w is the slot width. The yield point on the load-displacement experimental curve is (d_y, P_y) .

3.3.3 Effect of β and Δ on the average triaxiality

The "history output" included the equivalent plastic strain $\hat{\varepsilon}_p(t)$ as well as the pressures $\hat{P}(t) = -\frac{\sigma_{ii}}{3}$ and the von Mises stresses $\hat{\sigma}_{eq}(t)$ along the paths. The symbol t represent a time-like parameter that vary within the range $0 \le t \le 1$ while a hat symbol ^ represents average over all integration points of the elements adjacent to the paths. The triaxiality was calculated by : $\hat{t}_r(t) = \hat{P}(t) / \hat{\sigma}_{eq}(t)$ and presented as a function of $\hat{\varepsilon}_p(t)$. The triaxiality evolution with the applied load for β = -10°, 0°, 10°, 20° and 30° for Δ = 0.0 mm is shown in Fig. 9a. The results show that the higher the angle β the higher the triaxiality. It can also be observed that the triaxiality changes during loading. For β = -10° and 0° it becomes negative although it is initially positive. For β = 10° it remains quite constant with an approximate value of 0.25. For β = 20° the triaxiality increases slightly with the loading and climbs from an initial value of ~0.4 to ~0.6 at $\hat{\varepsilon}_p = 0.25$.

Higher increase of triaxiality can be obtained with β = 30°. The triaxiality is initially ~0.45 and reaches ~0.9 at $\hat{\varepsilon}_p = 0.25$.

The triaxiality evolution with the applied load for β = 0°, 10°, 20° and 30° for pre set of Δ = 0.75 mm is shown in Fig. 9b. It can be observed that the initial triaxiality is much higher than in Fig. 9a. For β = 0° and 10°, the triaxiality decreases with the load. The triaxiality remains rather constant for β = 20° with a quite high value of ~0.9. Since the yield stress of 4340 steel is 1400 MPa, this means that experiments with almost constant pressure of ~1260 MPa can be performed. For β = 30°, the triaxiality increases with the load from ~0.9 at $\hat{\varepsilon}_p = 0.01$ to ~1.15 at $\hat{\varepsilon}_p = 0.25$.

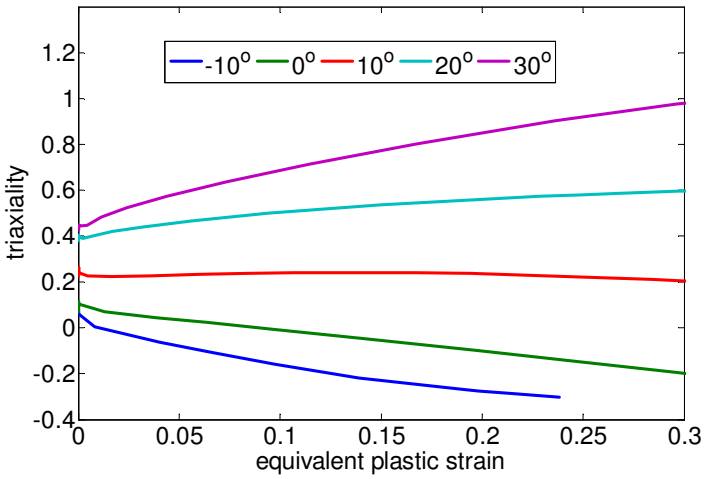

a.

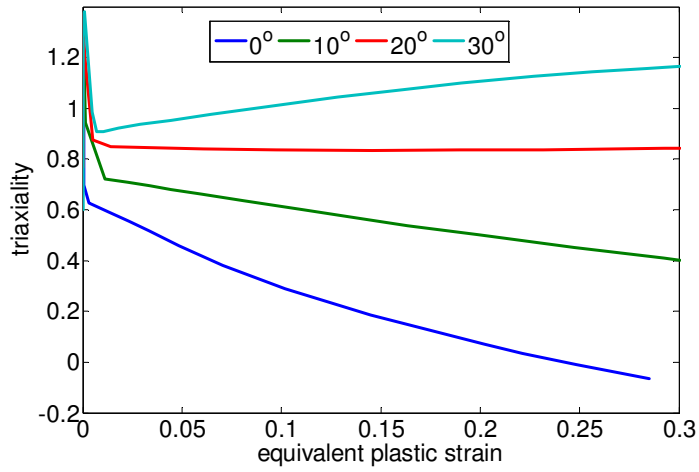

b.

Figure 9: The triaxiality evolution with the applied load. a. β = -10°, 0°, 10°, 20° and 30° for no pre set (Δ = 0.0 mm). b. β = 0°, 10°, 20° and 30° for pre set of Δ = 0.75 mm.

4. Experimental results

4.1 The materials

The numerical analyses presented above and preliminary tests were performed on five 4340 steel specimens in order to check the "limits" of our equipment and reach high pressures. Typical results of two tests performed with a 20° specimen will be presented here.

The body of the experimental results and their interpretation reported here are for five specimens made of Aluminum 7075 T651 with Young's modulus E=71.7 GPa, Poisson's ratio $\nu = 0.3$, and yield stress $\sigma_Y = 503\,\mathrm{MPa}$. This set of specimens and experimental parameters was designed in order to obtain a reasonably constant triaxiality during the main loading step.

4.2 The specimen geometry

For the present purpose of preliminary investigation four types of specimens were used in the experiments. The specimens differed only by the tilt angle β, namely $\beta = 0^o, 10^o, 15^o$ and 20^o. The inclination angle of the outer radii was chosen to be $\alpha = 85^o$ and the height of the specimen is 6 mm. The slot is 1 mm wide and 2 mm long in the vertical direction.

4.3 The experimental details

As mentioned above, tests were carried out with 4340 Q+T steel 50 HRC and 7075 T651. Experimental details are summarized in Table 1. The combinations of β and Δ for the 4340 steel were chosen to check the flow behavior under high triaxiality and pressures. For the aluminum the reasons were: 1. Evenly span the triaxiality levels between 0-1. 2. Obtain an approximately constant level of triaxiality during loading.

Table 1: Tests details.

Specimen	Material	β	Δ [mm]
S1	Steel 4340	20	0.0
S2	Steel 4340	20	0.75
S3	Aluminum 7075	0	0.0
S4	Aluminum 7075	10	0.0
S5	Aluminum 7075	15	0.0
S6	Aluminum 7075	15	0.5
S7	Aluminum 7075	20	0.75

4.4 Data reduction technique

The experimental results are load displacement (d-P) curves. These curves are analyzed to determine the *flow* stress-strain characteristic behavior as well as the fracture strain. This is done basically by a "trial and error" iterative technique. The procedure is done for each specimen type (β) in four steps which are detailed below:

1. For each specimen the test is simulated using the known elastic properties and assuming bi linear plastic model. The d-P curves due to different plastic moduli (E_p)are recorded.

2. The experimental d-P curves are compared to the numerical d-P curves which were obtained in step 1. The closest E_p is chosen and the coefficients k_1 and k_2 of Eqns (1)-(2) are generated from the numerical results for this E_p.

3. Eqns. (1)-(2) (with the obtained coefficients of step 2) and the experimental d-P curve are used to generate a "first guess" for the material characteristic $\sigma - \varepsilon$ curve. This curve is substituted into the numerical simulation and slightly modified by a "trial and error" technique until a satisfactory agreement between the numerical and experimental d-P

curves is obtained. The averaged field variables in the gauge are recorded to obtain the triaxiality during loading.

4. A "ductile failure" [1] criterion is added to numerical analysis and the resulting numerical d-P curve are compared to the experimental ones. The inputted equivalent plastic strain to the "ductile failure" criterion which causes fracture at the same point observed in the experimental d-P curve is the "fracture strain".

A detailed example of the data reduction technique, which involves several technicalities, is given in the supplementary material. It should be emphasized that the extraction of flow and fracture properties in what follows is brought for the sole purpose of demonstrating the efficiency of the proposed specimen.

4.5 Results

The experimental results and analyses of specimens made of 4340 steel and aluminum 7075 are given below.

4.5.1 4340 Steel

The raw load-displacements results of specimens S1 and S2 (table 1) are shown in figure 10. Specimen S2, which was pre-loaded up to $\Delta = 0.75\ mm$, sustain higher loads than S1 which was not pre-loaded. Both specimens did not fracture at the end of the test. Although damage started in early stages of the loading, the gauge did not break completely and the contact between the formed cracks within the gauge as well the contacting faces of the slots could maintain the applied load. The exact point on the experimental d-P curve at which damage initiated within the gauge cannot be pointed out exactly. Yet, the non-uniformity of the loading path may suggest damage accumulation of the gauge and slots. These points are marked with lines and correspond to unexpected increase of the measured load. It is quite clear that the results for displacements higher than 0.4 mm cannot be used since the load is not elevated because of the material

properties but because of geometrical changes caused by damage accumulation. Although the exact fracture strain can not be obtained by this 20^{o} specimen the effect of triaxiality on the flow properties can be obtained.

Application of the procedure described in section 4.4 resulted in the stress-strain curve shown in Fig. 11. A cylinder $6^{\phi} \times 6\ mm$ made of the same material was tested in compression and the results are compared to the results obtained here by the CSD specimens. The maximum stress of the shear specimen is 1960 MPa and that of the cylinder specimen 1810 MPa. The difference is ~8%. A fairly good agreement is observed, noting that compression tests of cylinders cannot generate the correct elastic properties which result in a much smaller slope in the elastic region.

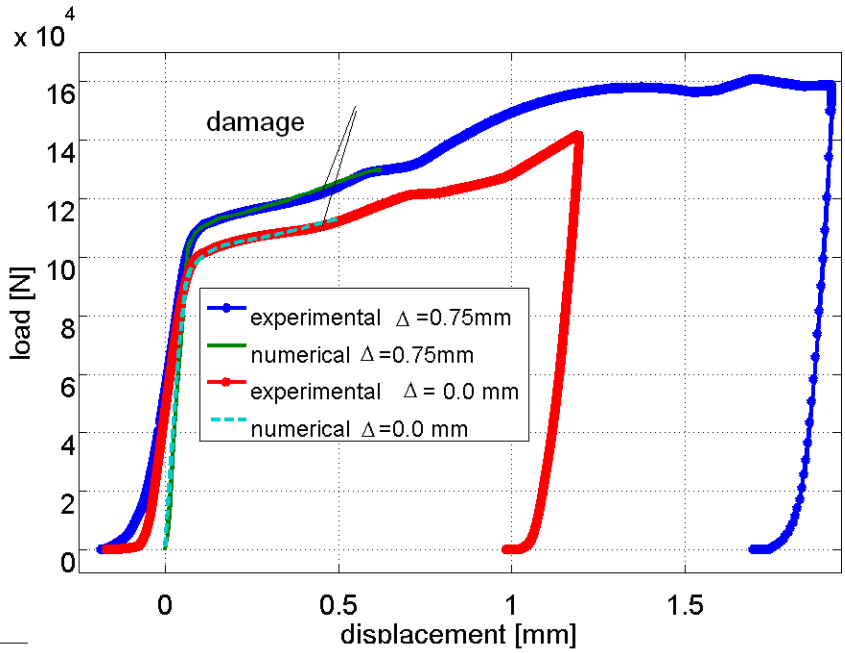

Figure 10: Experimental and numerical load displacement curves of the 4340 steel specimens

The $\sigma - \varepsilon$ of the shear specimen of Fig. 11 was used in the numerical simulation of the experiment and revealed a very good agreement with the raw data of the experiment, as shown by d-P curves in Fig. 10.

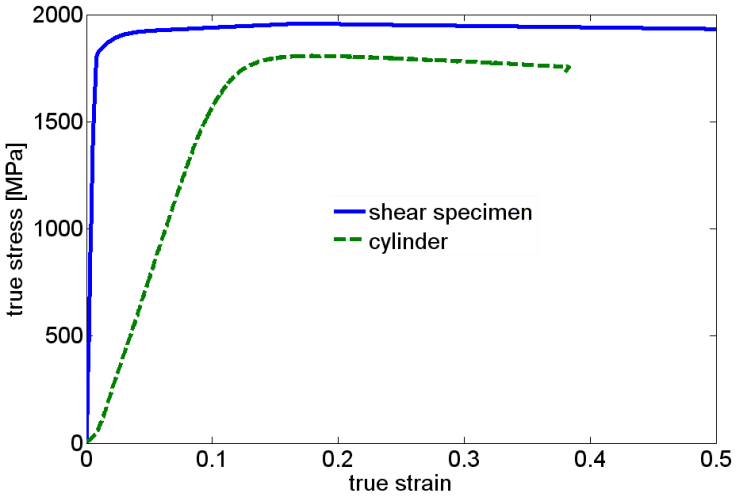

Figure 11: Resulting stress-strain curves due to shear specimens and cylindrical specimen.

The triaxiality during the test was calculated from the averaged stress on the mid line of the gauge, and typical results are shown in Fig. 12. Average values of tr = 0.41 and 0.72 are obtained for S1 and S2 respectively. Since the same $\sigma - \varepsilon$ was used to simulate successfully the d-P of both tests with different triaxialities, it means that the flow properties of 4340 are apparently insensitive to triaxiality (at least in the range tr = 0.41 - 0.7), corresponding to averaged pressures in the gauge $0.75 < P_{av} < 1.41$ GPa.

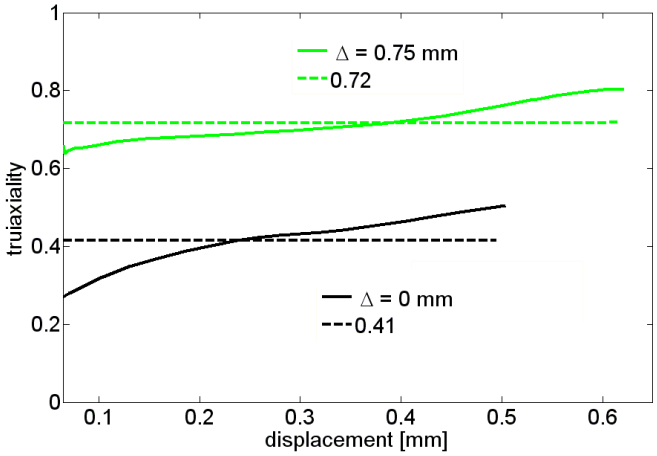

Figure 12: Triaxiality evolution during tests S1-S2 and their average values. Note that the pre load step of specimen S2 of $\Delta = 0.75$ *mm* introduces a higher triaxiality.

4.5.2 Aluminum 7075

The experimental load displacements curves, within the plastic range, for the five tests are shown in Fig. 13. The curves were shifted so that the zero displacements correspond to the estimated yield point. The end of each curve is the actual fracture point except for the specimen S7 with $\beta = 20^{o}$. An abrupt loss of bearing capacity in this specimen was not evident because of contact of the internal notch faces. The slightly oscillatory nature of the curve seen in Fig 13, at a displacement higher than 0.35, can be attributed to crack formation and propagation.

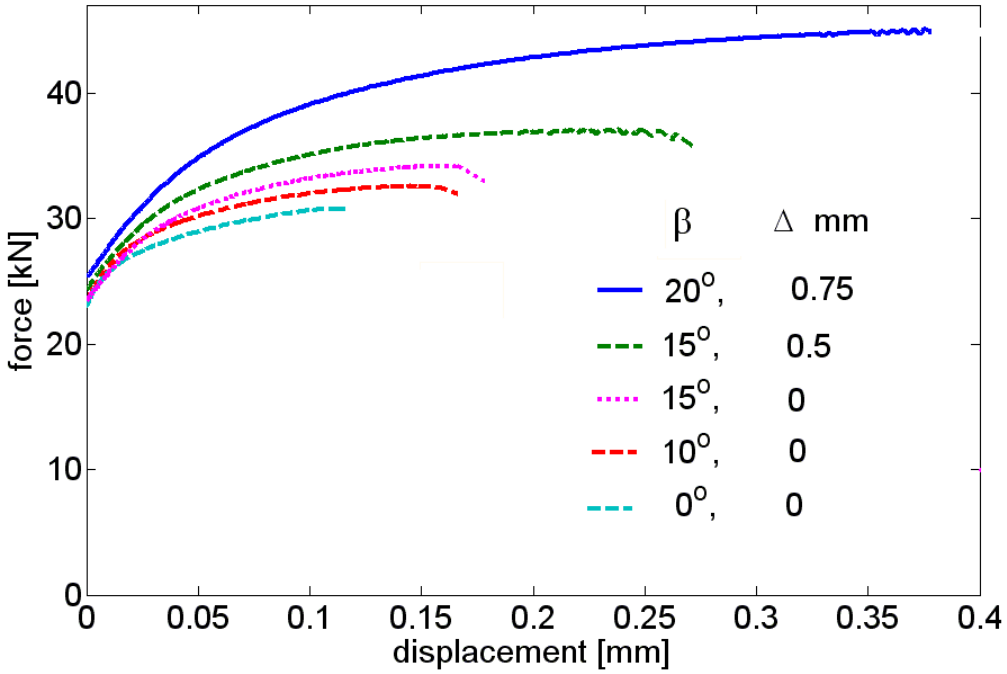

Figure 13: Experimental load displacement curves.

The characteristic triaxiality level of each experiment shown in Fig 13 was estimated during loading and given in Fig. 15. It can be observed that the higher the triaxiality the larger the attained displacement, which corresponds to larger plastic strains to fracture. Application of the data reduction technique of section 4.4 resulted in stress strain curves presented in Fig. 14. Validation of these curves is obtained by comparison to curves

obtained from compression of two $6^{\Phi} \times 6\ mm$ cylinders made of the same material. Their resulting $\sigma - \varepsilon$ curves are also included in Fig. 14. The good agreement between the results obtained by the shear specimens and the cylinders provide additional confidence in the suggested specimen.

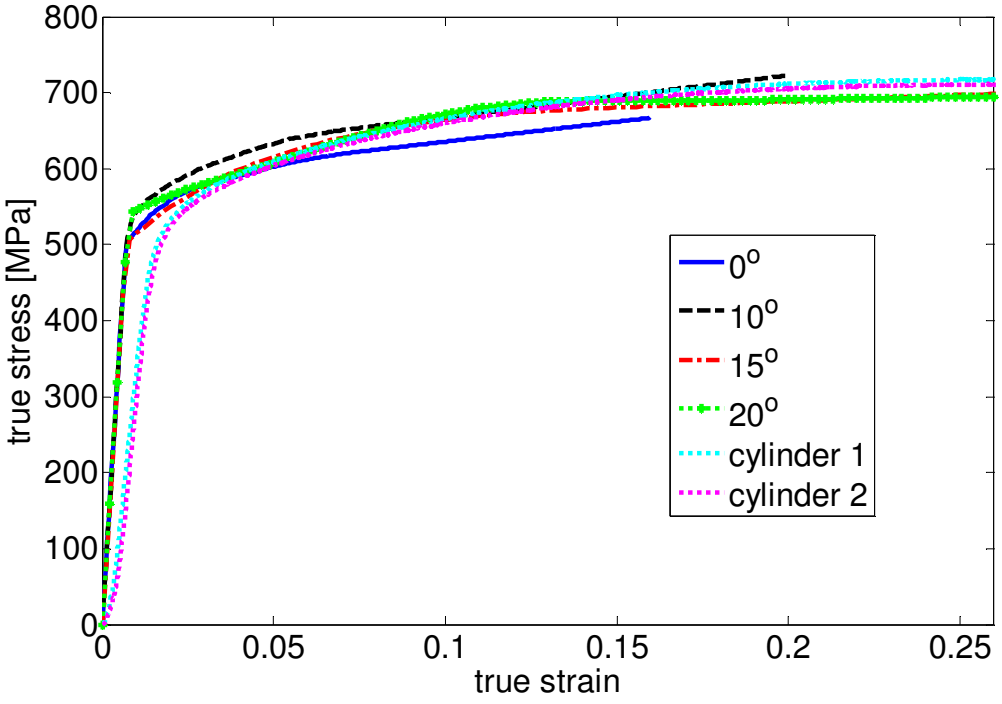

Figure 14: Obtained stress-strain curves for the aluminum 7075 T651 shear specimens and cylinders.

The evolution of the triaxiality and its average value are shown in Fig. 15. The averaged triaxiality values for tests S3 - S7 is : 0.06, 0.2, 0.41, 0.72 and 0.9 respectively. It can be observed that the stress-triaxiality is reasonably constant throughout the main loading step.

The fracture strain is calculated in step 4 of the data reduction technique detailed in section 4.4. This was done with Abaqus explicit [1] using the "ductile damage" with damage evolution option. Large solution times (~4 ms for the main loading step) were chosen to minimize the inertial effects. The experimental and numerical d-P curve of test S4 are shown in Fig. 16. The numerical results were obtained by applying the obtained

$\sigma - \varepsilon$ curves of Fig. 14. Numerical d-P curves for various plastic strains to fracture (0.15, 0.3, 05, 0.7 and 0.8) are shown as well. The explicit results are a bit more oscillatory because of the inertial effects. It can be observed that a plastic strain of 70% fits the fracture of test S6 which is done at tr = 0.72.

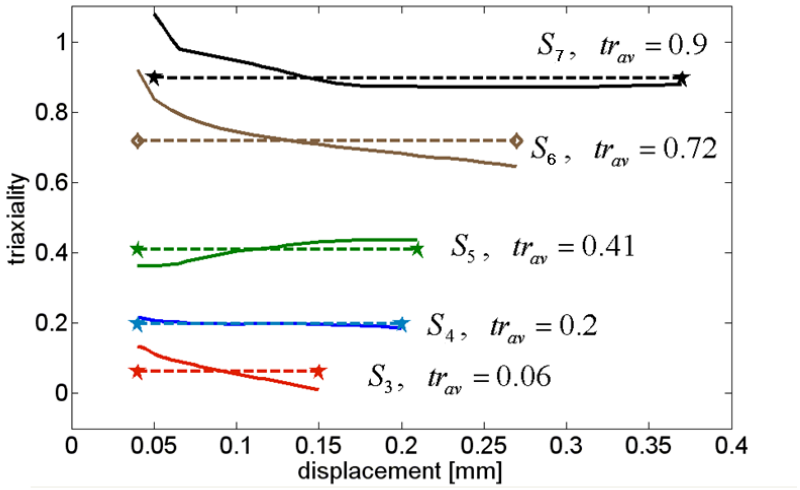

Figure 15: Triaxiality evolution during loading and triaxiality averages for the 5 tests of table 1.

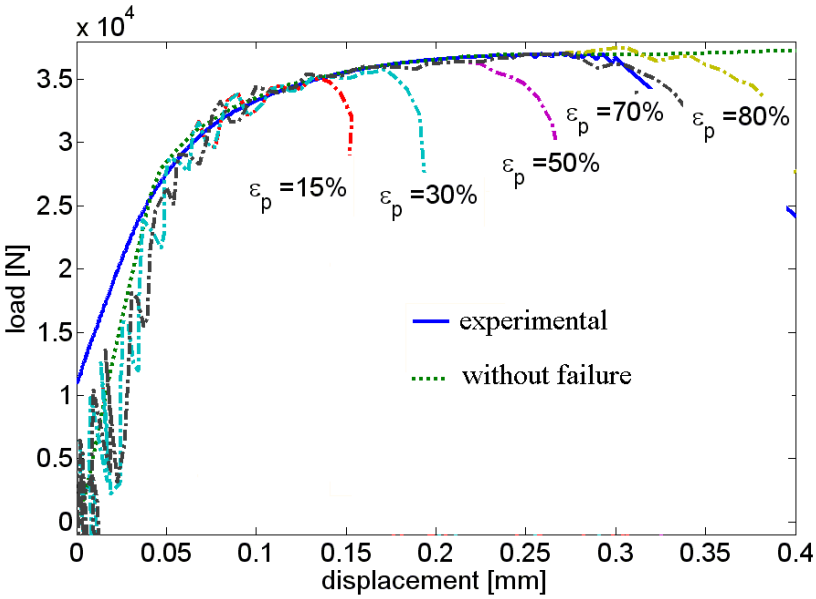

Figure 16: Comparison of experimental and numerical d-P curves with application of "ductile failure" criteria with 15%, 30%, 50%, 70% and 80% plastic strain to fracture, for test S4.

Fig. 17 summarizes the plastic strains to fracture versus triaxiality for the five tests. The triaxiality was calculated by two methods. The first one was obtained by applying implicit analysis which does not incorporate failure. This triaxiality which is shown in Fig. 15 was determined from the average stresses along the mid-line of the gauge. The second one uses the explicit analyses results which incorporate failure. The triaxiality is calculated as an average of the stresses in 15-20 elements which have failed at the specific plastic strain. The Johnson-Cook fracture model [13] is used. $\varepsilon_f^p\left(tr\right) = C_1 + C_2 \cdot \exp\left(C_3 \cdot tr\right)$.

Table 2: Johnson - Cook fracture parameters for aluminum 7075 T651.

coefficient	Implicit - no failure	***Explicit - failure***
C1	0.096	***0.045***
C2	0.049	***0.063***
C3	3.465	***3.384***

Failure is applied in the explicit analyses by deleting elements which have reached the limit value of the reported plastic strain. Hence recording the stresses of those elements and calculating their triaxiality evolution is a more accurate method for triaxiality calculation. But it can be observed that the differences between these two methods is small, probably due to the uniformity of the stresses within the gauge and the fact that most of the failed elements lie on the "working line", on which the stresses are calculated in the implicit analysis which does not incorporate failure. Bau and Wierzbicki (2004), [3] report on a cut-off value of the stress triaxiality equal to 1/3 (compression), above which fracture never occurs. This value was obtained by them empirically from upsetting tests. The present results do not reveal the existence of such a threshold.

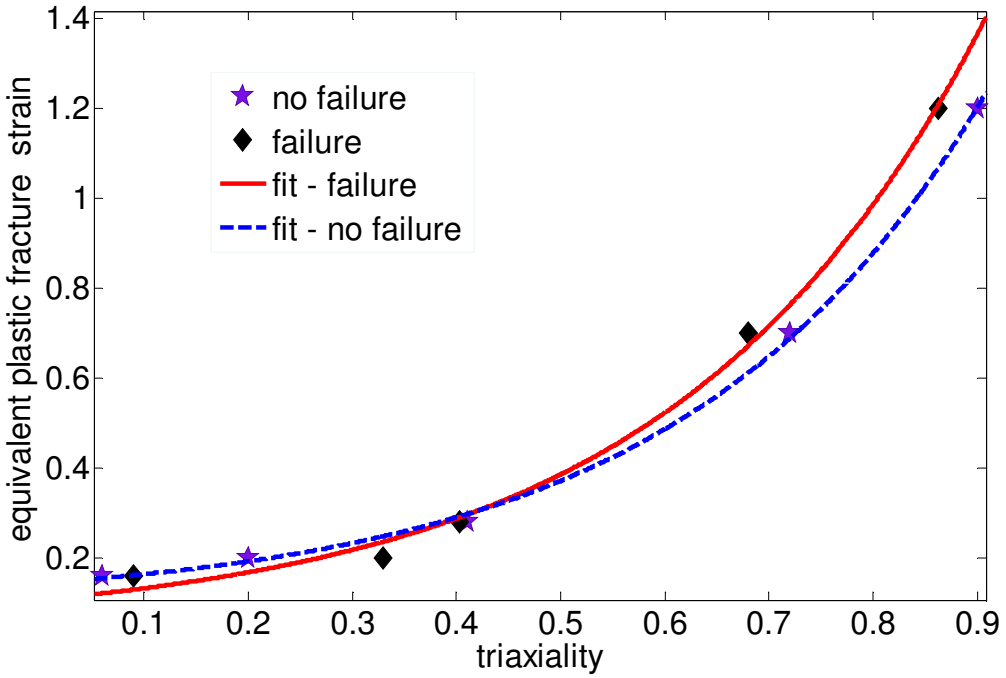

Figure 17: The obtained fracture strains for Aluminum 7075 T651 versus triaxiality. Results obtained by using tests S3-S7. Johnson-Cook [13] fracture model is fitted.

5. Discussion

The need for accurate determination of the flow and fracture properties of materials under varying levels of stress-triaxiality prompted this study in which a new specimen geometry and data reduction technique were developed. The specimen was thoroughly modeled numerically with the aim to investigate separately the influence of each controllable geometrical parameters on the confining pressure and stress triaxiality. The bottom line of the numerical study is that a variable and controllable degree of stress-triaxiality can be achieved with the main feature that the stress triaxiality is rather uniform in the gauge section. Another important feature of the specimen is the capacity to smoothly address both positive and negative stress-triaxialities, even if negative (tensile) ones are still of a limited extent. The specimen and the data reduction technique were applied to quasi-static loading cases but it can reasonably be proposed that this concept will equally well apply to the dynamic regime, thus bridging a large range of strain rates in a seamless manner, with a single specimen geometry. This overcomes the need to "patch" data

obtained from various experimental configurations. Yet, as discussed in the introduction, the proposed technique relies heavily on numerical simulations to identify the flow and failure parameters of the investigated material. The overall numerical procedure is not complicated and requires an initial guess followed by an iterative process in which the load-displacement curves are reproduced to a satisfactory extent. While a purely analytical approach might have been preferable and would have been more straightforward, the problem at hand does not lend itself to a straightforward simple analytical solution, so that the practicing engineer will need to apply some numerical calculations to process the measured data. This kind of situations is not new in experimental mechanics, and almost all the techniques which were proposed in the recent years to investigate this and related issues all rely on a hybrid experimental-numerical approach.

Past the initial modeling and characterization of the specimen, some experimental tests were carried out to confirm the overall approach proposed here. Preliminary tests were carried out on 4340 Q+T (50 HRC) steel specimens, but the main body of experiments were carried out on 7075-T651 aluminum alloy. The main purpose of the experiments was to demonstrate the feasibility to extract with a reasonable effort and accuracy the material properties under various controlled triaxiality conditions. The same purpose was behind the detailed analysis of the two materials used in the experiments. These preliminary experiments and analysis seem to support the Johnson-Cook failure criterion [15] and they also pave the way for a systematic investigation of other types of materials, including the more brittle or pressure-sensitive ones using the SCD suggested here.

Finally, the next part of the investigation, under current consideration, is the extension of the proposed methodology to dynamic characterization of the mechanical and failure properties.

It is believed that the proposed methodology is enticing for the practitioners because of its overall simplicity and should open the way for more routine-type of characterizations of the mechanical and failure properties of engineering materials.

6. Conclusions

- A new methodology for testing the flow and failure properties of materials subjected to a stress- triaxiality $-0.2 < t_r < 1.2$ was successfully developed.
- The specimen (Shear Compression Disk) consists of a truncated conical slotted disk which is inserted into a confining sleeve.
- The measured load-displacement data is reduced into equivalent stress-strain data using a hybrid experimental-numerical procedure.
- The numerical study shows a constant level of stress triaxiality that can be controlled through the choice of geometrical parameters.
- Quasi-static experimental results were reported for 4340 Q+T steel and 7075-T651aluminum alloy.
- The experimental results support the proposed methodology.

7. Acknowledgement

Financial support from Vatat (2013152) is greatly acknowledged. The authors wish to thank A. Amon and A. Reuven (Materials Mechanics Center) for their dedicated technical assistance.

References

[1] Abaqus/CAE 6.9-EF1 (2009) Finite element package Dassault Systemes Simulia corp.Providence, RI, USA.

[2] Alves M, Jones N (1999) Infuence of hydrostatic stress on failure of axisymmetric notched specimens. J MechH Phys Solids 47: 643-667

[3] Bao Y, Wierzbicki T (2004) A comparative study on various ductile crack formation criteria. J Eng Mater-T ASME 126:315-324

[4] Bridgman PW (1952) Studies in Large Plastic Flow and Fracture with Special Emphasis on the Effects of Hydrostatic Pressure. McGraw-Hill, New York

[5] Brünig M, Chyra O, Albrecht D, Driemeier L, Alves M (2008) A ductile damage criterion at various stress triaxialities. Int J Plasticity 24:1731–1755

[6] Che HY, Zhu L, Sun DZ, Chen JH, Zhu H (2007) Characterization and modeling of aluminum extrusion damage under crash loading. Thin Wall Struct 45: 383-392

[7] Couque H (2003) A hydrodynamic hat specimen to investigate pressure and strain rate dependence on adiabatic shear band formation. Journal de Physique IV 110: 423-428

[8] Couque H (2005) Dynamic compression failure of two metals at 0.5 and 1.5 GPa. Computational Ballistics II 2005. WIT Press 239-248
[9] Dorogoy A, Rittel D (2005) Numerical validation of the shear compression specimen. Part I: quasi-static large strain testing. Exp Mech 45(2): 167-177
[10] Ferguson WG, Hauser FE, Dorn JE (1967) Dislocation damping in zinc single crystals. Brit J Appl Phys 18:411:417
[11] Gu Y, Nesterenko VF (2007) Dynamic behavior of HIPed Ti–6Al–4V. Int J Impact Eng 34:771–783
[12] Guduru RK, Darling KA, Scattergood RO, Koch CC, Murty KL (2007) Mechanical properties of electrodeposited nanocrystalline copper using tensile and shear punch tests. J Mater Sci 42:5581–5588
[13] Hopperstad OS, Børvik T, Langseth M, Labibes K, Albertini C (2003) On the influence of stress triaxiality and strain rate on the behaviour of a structural steel Part I: Experiments. Eur J Mech A-Solid 22:1–13
[14] Hancock JW, Mackenzie AC (1976) On the mechanisms of ductile failure in hig-strength steels subjected to multi-axial stress-states. J Mech Phys Solids 24: 147-169
[15] Johnson G, Cook W (1985) Fracture characteristics of three metals subjected to various strains, strain rates and temperatures. Eng Fract Mech 21: 31-48
[16] Klepaczko JR (2001) Remarks on impact shearing. J Mech Phys Solids 46(10): 1028-1042
[17] Larose J, Lewandowski JJ (2002) Pressure effects on flow and fracture of Be-Al alloys. Metall Mater Trans A 33A: 3555- 3564
[18] Lewandowski JJ, Lowhaphandu P (1998) Effects of hydrostatic pressure on mechanical behaviour and deformation processing of materials. Int Mater Rev 43(4):145-187
[19] Li QM, Jones N (2002) Response and failure of a double-shear beam subjected to mass impact. Int J Solids Struct 39: 1919–1947
[20] Mae H (2009) Characterization of material ductility of PP/EPR/talc blend under wide range of stress triaxiality at intermediate and high strain rates. J Appl Polim Sci 111: 854–868
[21] Meyer LW, Manwaring S (1986) Critical adiabatic shear strength of low alloyed steel under compressive loading. Metallurgical applications of shock-wave and high-strain-rate phenomena. Marcel Dekker, Inc, New York, NY, 657–673
[22] Mirone G (2007) Role of stress triaxiality in elastoplastic characterization and ductile failure prediction. Eng Fract Mech 74:1203-1221.
[23] Mirone G (2008) Elastoplastic characterization and damage predictions under evolving local triaxiality: axysimmetric and thick plate specimens. Mech Mater 40: 685–694
[24] Mishra A, Martin M, Thadhani NN, Kad BK, Kenik EA, Meyers MA (2008) High-strain-rate response of ultra-fine-grained copper. Acta Mater 56: 2770–2783
[25] Rittel D, Lee S, Ravichandran G (2002) A shear compression specimen for large strain testing. Exp Mechs 42:58-64
[24] Rusinek A, Klepaczko JR (2001) Shear testing of a sheet steel at wide range of strain rates and a constitutive relation with strain-rate and temperature dependence of the flow stress. Int J Plasticity17:87-115

[25] Yu MH (2004) Unified Strength Theory and its Applications. Springer.